Photon statistics of two-mode squeezed states and interference in four-dimensional phase space

Carlton M. Caves and Chang Zhu
Center for Laser Studies, University of Southern California, Los Angeles, California 90089-1112

G. J. Milburn
Department of Physics, University of Queensland, St. Lucia, Queensland 4067, Australia

W. Schleich
Max-Planck-Institut für Quantenoptik, D-8046 Garching bei München, Federal Republic of Germany
(Received 1 October 1990)

We derive the joint photon-number distribution for two-mode squeezed states with coherent amplitudes. For certain ranges of the parameters, the joint distribution exhibits nonclassical oscillations, which are the two-mode analog of the oscillations found in the single-mode case. These nonclassical oscillations are absent from the marginal distributions for each mode. The nonclassical features of the joint distribution may be explained using the interference–in–phase-space concept in four-dimensional phase space.

I. INTRODUCTION

The photon-number probability distribution of a single-mode squeezed state[1] has been studied by several authors.[2–5] If the parameters of the squeezed state are chosen appropriately, the photon-number distribution can exhibit nonclassical oscillations,[3] which are now well understood in terms of "interference in phase space."[3–5] In Sec. II we derive the joint photon-number probability distribution for two-mode squeezed states[6] and show that for particular choices of parameters there are similar nonclassical oscillations in the joint distribution. In Sec. III an analysis of the joint photon-number distribution reveals that these oscillations may be interpreted as due to interference in four-dimensional phase space.

The oscillations in the joint photon-number distribution might be observed in experiments that generate *pulsed* two-mode squeezed light. In previous experiments of this sort,[7,8] the pulses of two-mode squeezed light were generated by an optical parametric amplifier, and the two correlated modes (signal and idler) had orthogonal polarizations. This last feature is not essential, however, and in other configurations the two modes might be distinguished by frequency or by propagation direction. Having separated the two modes, as was done by using a polarizing beamsplitter in the most recent experiment,[8] one could direct them onto separate photocounters and then build up the joint photon-number distribution from the photocount statistics of a sequence of pulses. Of course, the oscillations would be very difficult to observe in practice, because the subunity quantum efficiency of available photocounters reduces their visibility, as has been demonstrated in the single-mode case by Milburn and Walls.[9] The prospects for observing the oscillations in continuous-wave, as opposed to pulsed, two-mode squeezed light are even worse, because effective inefficiencies and multimode effects in direction detection of continuous-wave squeezed light are likely to render the oscillations invisible, even for photocounters with unity quantum efficiency. These effects have been investigated recently for the single-mode case by Zhu and Caves.[10]

II. PHOTON-NUMBER DISTRIBUTION FOR TWO-MODE SQUEEZED STATES

Consider two modes of the electromagnetic field, which have annihilation operators $\hat{a}_1$ and $\hat{a}_2$. An ideal two-mode squeezed state[6] is defined by

$$|\alpha_1,\alpha_2\rangle_{(r,\phi)} \equiv \hat{D}(\alpha_1,\alpha_2)\hat{S}(r,\phi)|0\rangle \ , \tag{2.1}$$

where $|0\rangle$ is the two-mode vacuum state. The two-mode squeeze operator,[6]

$$\hat{S}(r,\phi) \equiv \exp\left[r(\hat{a}_1\hat{a}_2 e^{-2i\phi} - \hat{a}_1^\dagger \hat{a}_2^\dagger e^{2i\phi})\right] \ , \tag{2.2}$$

is characterized by a (real) squeeze parameter r and an angle ϕ that determines the phase of the squeezing. The two-mode displacement operator,

$$\hat{D}(\alpha_1,\alpha_2) \equiv \hat{D}_1(\alpha_1)\hat{D}_2(\alpha_2) \ , \tag{2.3}$$

is a product of displacement operators for each mode,

$$\hat{D}_i(\alpha_i) \equiv \exp(\alpha_i \hat{a}_i^\dagger - \alpha_i^* \hat{a}_i) \ , \quad i=1,2 \ , \tag{2.4}$$

where $\alpha_i = \langle \hat{a}_i \rangle$ is the coherent amplitude of mode i. Without loss of generality, we may set the squeezing phase $\phi = 0$ in what follows.

The joint probability to find n_1 photons in mode 1 and n_2 photons in mode 2 is given by

$$P(n_1,n_2)=|\langle n_1,n_2|\alpha_1,\alpha_2\rangle_{(r,0)}|^2 , \tag{2.5}$$

where $|n_1,n_2\rangle \equiv |n_1\rangle_1 \otimes |n_2\rangle_2$ is the direct product of photon-number eigenstates $|n_1\rangle_1$ and $|n_2\rangle_2$ for modes 1 and 2. The mean number of photons in the two-mode squeezed state is[6]

$$\langle \hat{a}_1^\dagger \hat{a}_1 + \hat{a}_2^\dagger \hat{a}_2\rangle = |\alpha_1|^2 + |\alpha_2|^2 + 2\sinh^2 r , \tag{2.6}$$

where $|\alpha_i|^2$ is the mean number of coherent photons in mode i and $2\sinh^2 r$ is the mean number of photons resulting from the squeezing.

To calculate the probability amplitude

$$c(n_1,n_2) \equiv \langle n_1,n_2|\alpha_1,\alpha_2\rangle_{(r,0)} , \tag{2.7}$$

we proceed by an appropriate operator ordering of the two-mode displacement and squeeze operators. The two-mode squeeze operator may be written as[6]

$$\hat{S}(r,0) = \frac{1}{\cosh r} e^{-\hat{a}_1^\dagger \hat{a}_2^\dagger \tanh r} \times e^{-(\hat{a}_1^\dagger \hat{a}_1 + \hat{a}_2^\dagger \hat{a}_2)\ln(\cosh r)} e^{\hat{a}_1 \hat{a}_2 \tanh r} . \tag{2.8}$$

When this form of $\hat{S}(r,0)$ acts on the vacuum state, the second and third exponentials may be replaced by unity, leaving the amplitude (2.7) in the form

$$c(n_1,n_2) = \frac{1}{\cosh r}\langle n_1,n_2|\hat{D}_1(\alpha_1)\hat{D}_2(\alpha_2)e^{-\hat{a}_1^\dagger \hat{a}_2^\dagger \tanh r}|0\rangle . \tag{2.9}$$

Moving the displacement operators through the squeeze operator and then normal ordering the displacement operators, we find

$$c(n_1,n_2) = \frac{e^{-(\alpha_1^*\mu_1+\alpha_2^*\mu_2)/2}}{\cosh r}\langle n_1,n_2|e^{-\hat{a}_1^\dagger \hat{a}_2^\dagger \tanh r} e^{\mu_1 \hat{a}_1^\dagger} e^{\mu_2 \hat{a}_2^\dagger}|0\rangle , \tag{2.10}$$

where we define

$$\mu_1 \equiv \alpha_1 + \alpha_2^* \tanh r , \tag{2.11}$$

$$\mu_2 \equiv \alpha_2 + \alpha_1^* \tanh r . \tag{2.12}$$

Expanding the exponentials in Eq. (2.10), we are able to write the matrix element on the right as

$$\sqrt{n_1!\,n_2!}\,\mu_1^{n_1}\mu_2^{n_2} \sum_{j=0}^{\min(n_1,n_2)} \frac{1}{j!\,(n_1-j)!\,(n_2-j)!}\left(-\frac{\mu_1\mu_2}{\tanh r}\right)^{-j} . \tag{2.13}$$

The index j is the number of pairs of photons created by $e^{-\hat{a}_1^\dagger \hat{a}_2^\dagger \tanh r}$, whereas $n_1 - j$ and $n_2 - j$ are the numbers of photons created singly by $e^{\mu_1 \hat{a}_1^\dagger}$ and $e^{\mu_2 \hat{a}_2^\dagger}$. The sum in Eq. (2.13) may be manipulated into a form that involves a generalized Laguerre polynomial $L_n^{(\alpha)}(x)$. We are thus able to put the amplitude (2.7) into its final form

$$c(n_1,n_2) = \frac{(-\tanh r)^p}{\cosh r}\left(\frac{p!}{q!}\right)^{1/2} \mu_1^{n_1-p}\mu_2^{n_2-p} L_p^{(q-p)}\left(\frac{\mu_1\mu_2}{\tanh r}\right) e^{-(\alpha_1^*\mu_1+\alpha_2^*\mu_2)/2} , \tag{2.14}$$

where

$$p \equiv \min(n_1,n_2) , \tag{2.15}$$

$$q \equiv \max(n_1,n_2) . \tag{2.16}$$

The elements of the joint distribution (2.5) along the main diagonal $n_1 = n_2 = n$ are given by

$$P(n,n) = \frac{(\tanh r)^{2n}}{\cosh^2 r}\left| L_n^{(0)}\left(\frac{\mu_1\mu_2}{\tanh r}\right)\right|^2 \exp\left\{-[|\alpha_1|^2 + |\alpha_2|^2 + (\alpha_1\alpha_2 + \alpha_1^*\alpha_2^*)\tanh r]\right\} . \tag{2.17}$$

When there are no coherent amplitudes—i.e., $\alpha_1 = \alpha_2 = 0$—the joint distribution

$$P(n_1,n_2) = P(n,n)\delta_{n_1,n}\delta_{n_2,n} \tag{2.18}$$

has only diagonal elements

$$P(n,n) = \frac{(\tanh r)^{2n}}{\cosh^2 r} , \tag{2.19}$$

a result obtained previously.[6]

In Figs. 1–3 we plot diagonal and/or joint photon-number distributions for three two-mode squeezed states. In Fig. 1 the state is specified by $\alpha_1 = \alpha_2 = 3.0$ (both real) and $r = 1.5$. Clearly evident in both the diagonal distribution [Fig. 1(a)] and the joint distribution [Fig. 1(b)] are oscillations that are similar to the oscillations in the high-number tail of the photon-number

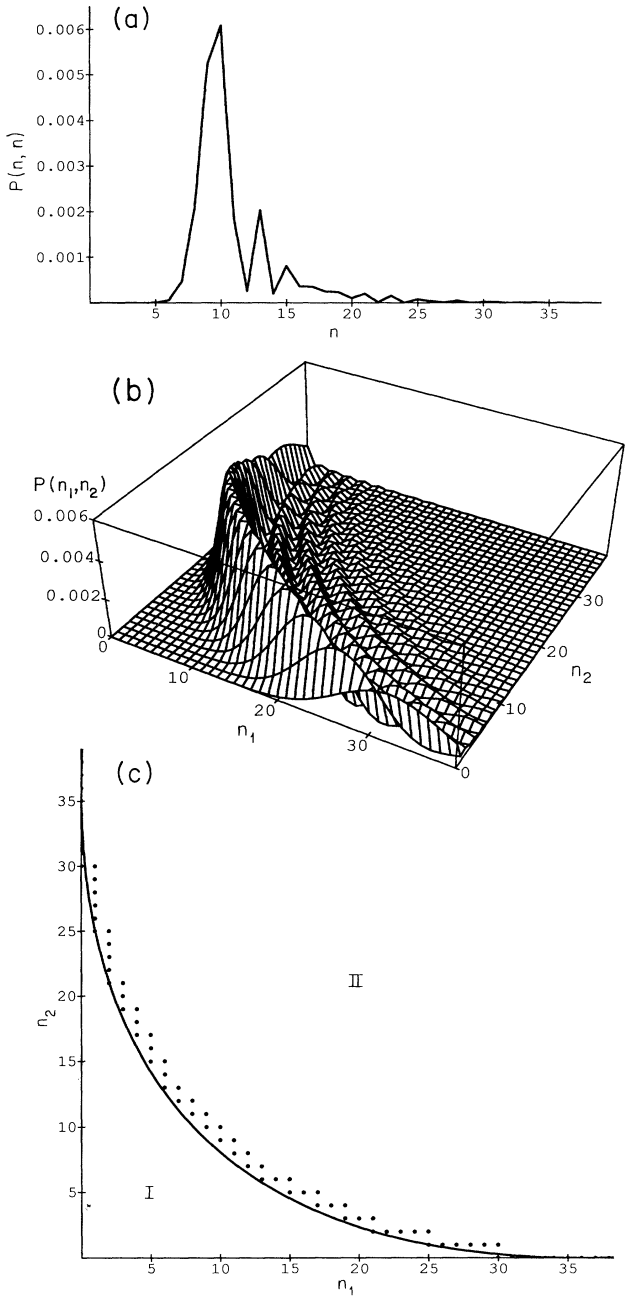

FIG. 1. Photon-number probabilities for a two-mode squeezed state $|\alpha_1, \alpha_2\rangle_{(r,0)}$ [Eq. (2.1)] with $\alpha_1 = \alpha_2 = 3.0$ and $r = 1.5$. For this state there are on average 18 coherent photons (9 in each mode) and $\simeq 9.07$ squeezed photons. (a) Diagonal joint distribution $P(n, n)$ [Eq. (2.17)]. There are obvious oscillations beyond the first maximum. (b) Three-dimensional plot of the joint distribution $P(n_1, n_2)$ [Eq. (2.5)]. There are obvious oscillations beyond the first maximum; peaks of successive maxima lie on the main diagonal. (c) The parabola (3.25) and regions I and II [Eqs. (3.22) and (3.23)] for this state, which has $X_0 = 6\sqrt{2} \simeq 8.49$. (region III lies almost entirely outside the area graphed.) The parabola approximates the first maximum of $P(n_1, n_2)$. The dots mark the actual position of the first maximum, determined by moving out from the n_1 or n_2 axis along a diagonal until the first maximum is reached.

distribution for single-mode squeezed states.[3] Successive maxima of the joint distribution appear to lie on parabolas symmetric about the main diagonal $n_1 = n_2$. In Fig. 2 the state is specified by $\alpha_1 = -\alpha_2 = 3.0$ and $r = 1.5$. There are no oscillations in either the diagonal distribution [Fig. 2(a)] or the joint distribution [Fig. 2(b)]. In Fig. 3 the state is specified by $\alpha_1 = 0$, $\alpha_2 = \sqrt{18} \simeq 4.24$, and $r = 1.5$. The joint distribution [Fig. 3(a)] has oscillations with much the same structure as in Fig. 1(b), except that the peaks of the maxima are shifted to the n_2 axis. The features of these distributions—including the parabolic shape of the maxima in Figs. 1(b) and 3(a) and the absence of oscillations in Fig. 2—are most easily explained using the concept of interference in phase space, to which we turn in Sec. III.

Before turning to interference in phase space, however, we consider briefly the marginal probability $P_1(n_1)$ to find n_1 photons in mode 1. Although this distribution may be derived by summing the joint distribution $P(n_1, n_2)$ over n_2, we calculate it here by a different method. The reduced density operator $\hat{\rho}_1$ for mode 1 is obtained as a partial trace over mode 2:

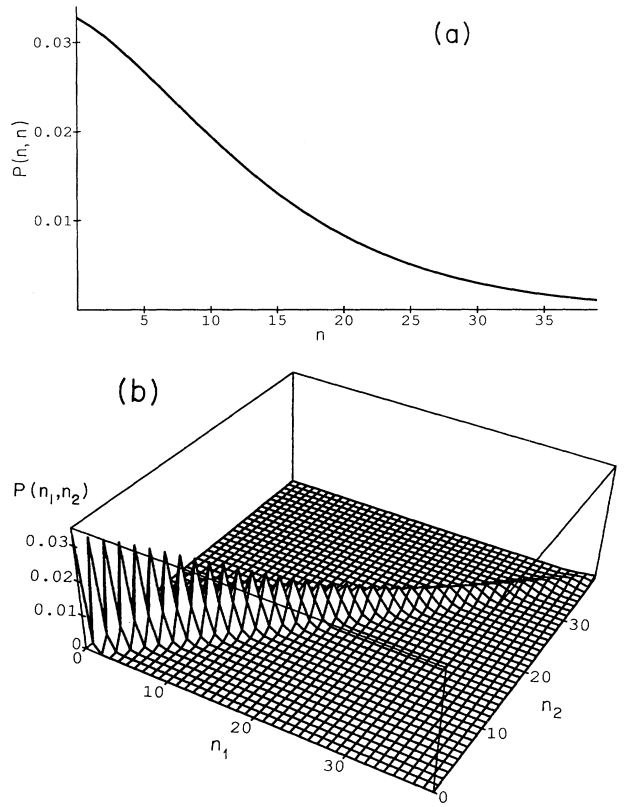

FIG. 2. Photon-number probabilities for a two-mode squeezed state $|\alpha_1, \alpha_2\rangle_{(r,0)}$ [Eq. (2.1)] with $\alpha_1 = -\alpha_2 = 3.0$ and $r = 1.5$. For this state there are on average 18 coherent photons (9 in each mode) and $\simeq 9.07$ squeezed photons. (a) Diagonal joint distribution $P(n, n)$ [Eq. (2.17)]. There are no oscillations. (b) Three-dimensional plot of the joint distribution $P(n_1, n_2)$ [Eq. (2.5)]. The distribution is concentrated near the main diagonal, and there are no oscillations.

$$\hat{\rho}_1 = \mathrm{tr}_2\left(|\alpha_1,\alpha_2\rangle_{(r,0)\,(r,0)}\langle\alpha_1,\alpha_2|\right) = \int \frac{d^2\beta_2}{\pi}\, {}_2\langle\beta_2|\alpha_1,\alpha_2\rangle_{(r,0)\,(r,0)}\langle\alpha_1,\alpha_2|\beta_2\rangle_2 \,. \tag{2.20}$$

Here the trace over mode 2 is carried out as an integral over the coherent states $|\beta_2\rangle_2$ of mode 2. We now substitute into Eq. (2.20) the two-mode squeezed state (2.1), write the two-mode squeeze operator in the form (2.8), carry out some tedious algebra involving coherent states and displacement operators, and finally write the reduced density operator as an incoherent mixture of coherent states $|\beta_1\rangle_1$ for mode 1,

$$\hat{\rho}_1 = \int d^2\beta_1\, P_1(\beta_1)|\beta_1\rangle_1\,{}_1\langle\beta_1| \,, \tag{2.21}$$

where the P function for mode 1,

$$P_1(\beta_1) = \frac{1}{\pi \sinh^2 r} \exp\left(-\frac{|\beta_1-\alpha_1|^2}{\sinh^2 r}\right) , \tag{2.22}$$

is that of a displaced thermal state.[11] The displaced thermal state has a mean number of photons $\sinh^2 r$, half the average number of squeezed photons, and it is displaced by α_1 in its phase plane.

That the reduced state of mode 1 has a P function means that it is a classical state; there should be no nonclassical oscillations in its photon-number distribution $P_1(n_1)$. Perhaps the easiest way to get at $P_1(n_1)$ is to calculate first the photon-number generating function,

$$\begin{aligned} Q_1(\lambda_1) &\equiv \sum_{n_1}(1-\lambda_1)^{n_1} P_1(n_1) \\ &= \mathrm{tr}_1\left(\hat{\rho}_1 {:}e^{-\lambda_1 \hat{a}_1^\dagger \hat{a}_1}{:}\right) \\ &= \frac{1}{1+\lambda_1 \sinh^2 r} \exp\left(-\frac{\lambda_1|\alpha_1|^2}{1+\lambda_1\sinh^2 r}\right) , \end{aligned} \tag{2.23}$$

and then to invert $Q_1(\lambda_1)$ by using a generating function for Laguerre polynomials,[12]

$$\begin{aligned} P_1(n_1) = &\frac{(\tanh r)^{2n_1}}{\cosh^2 r}\, L_{n_1}\left(-\frac{|\alpha_1|^2}{\cosh^2 r \sinh^2 r}\right) \\ &\times \exp\left(-\frac{|\alpha_1|^2}{\cosh^2 r}\right) , \end{aligned} \tag{2.24}$$

where $L_{n_1}(x) = L_{n_1}^{(0)}(x)$ is an ordinary Laguerre polynomial. The marginal distribution (2.24) does not exhibit any oscillations.

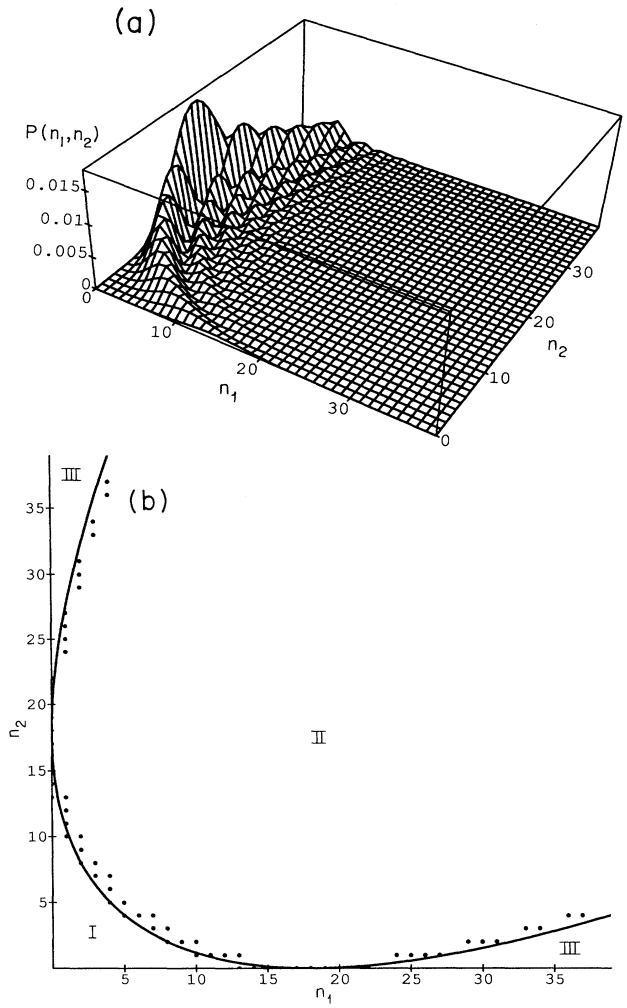

FIG. 3. Photon-number probabilities for a two-mode squeezed state $|\alpha_1,\alpha_2\rangle_{(r,0)}$ [Eq. (2.1)] with $\alpha_1 = 0$, $\alpha_2 = \sqrt{18} \simeq 4.24$, and $r = 1.5$. For this state there are on average 18 coherent photons (none in mode 1 and 18 in mode 2) and $\simeq 9.07$ squeezed photons. (a) Three-dimensional plot of the joint distribution $P(n_1,n_2)$ [Eq. (2.5)]. There are oscillations with much the same structure as in Fig. 1(b), except that the peaks of the successive maxima are shifted toward the n_2 axis. (b) The parabola (3.25) and regions I, II, and III [Eqs. (3.22)–(3.24)] for this state, which has $X_0 = 6$. The parabola approximates the first maximum of $P(n_1,n_2)$. The dots mark the actual position of the first maximum, determined by moving out from the n_1 or n_2 axis along a diagonal until the first maximum is reached.

III. INTERFERENCE IN FOUR-DIMENSIONAL PHASE SPACE

One expects on the basis of the analyses in Refs. 3 and 5 that the oscillations in the joint photon-number distribution may be interpreted in terms of interference in phase space. We now show that this is indeed the case. Moreover, the analysis predicts the form of the first curve of maximum probability in the n_1-n_2 plane.

We begin by writing the photon-counting probability amplitude (2.7) in terms of configuration space wave functions,

$$c(n_1,n_2)=\int_{-\infty}^{\infty}dx_1\int_{-\infty}^{\infty}dx_2\,U_{n_1}(x_1)U_{n_2}(x_2)\langle x_1,x_2|\alpha_1,\alpha_2\rangle_{(r,0)}\ , \tag{3.1}$$

where

$$U_{n_i}(x_i)\equiv\langle x_i|n_i\rangle=\langle n_i|x_i\rangle \tag{3.2}$$

is the (real) eigenfunction for an oscillator number state with n_i quanta. The coordinate wave function for a two-mode squeezed state is given by[13]

$$\langle x_1,x_2|\alpha_1,\alpha_2\rangle_{(r,0)}=\frac{e^{i\delta/2}}{\sqrt{\pi}}\exp\left(-\frac{i}{2}\mathbf{p}_0^{\mathrm{T}}\mathbf{x}_0\right)\exp(i\mathbf{p}_0^{\mathrm{T}}\mathbf{x})\exp\left(-\frac{1}{2}(\Delta\mathbf{x})^{\mathrm{T}}\underline{M}\Delta\mathbf{x}\right)\ , \tag{3.3}$$

where δ is an irrelevant phase that we set to zero henceforth. The wave function (3.3) is written in vector notation, with

$$\mathbf{x}\equiv\begin{pmatrix}x_1\\x_2\end{pmatrix}\ . \tag{3.4}$$

The mean positions and momenta are also written in this vector notation:

$$\mathbf{x}_0\equiv\begin{pmatrix}\langle x_1\rangle\\\langle x_2\rangle\end{pmatrix}=\sqrt{2}\begin{pmatrix}\mathrm{Re}(\alpha_1)\\\mathrm{Re}(\alpha_2)\end{pmatrix}\ , \tag{3.5}$$

$$\mathbf{p}_0\equiv\begin{pmatrix}\langle p_1\rangle\\\langle p_2\rangle\end{pmatrix}=\sqrt{2}\begin{pmatrix}\mathrm{Im}(\alpha_1)\\\mathrm{Im}(\alpha_2)\end{pmatrix}\ . \tag{3.6}$$

The wave function is completed by defining

$$\Delta\mathbf{x}\equiv\mathbf{x}-\mathbf{x}_0 \tag{3.7}$$

and by specifying the matrix

$$\underline{M}\equiv\begin{pmatrix}\cosh 2r & \sinh 2r\\ \sinh 2r & \cosh 2r\end{pmatrix}\ , \tag{3.8}$$

which is half the inverse of the coordinate covariance matrix. For simplicity we take α_1 and α_2 to be real henceforth; this implies that $\mathbf{p}_0=0$.

We now change variables to diagonalize $\underline{M}$:

$$X\equiv x_1+x_2\ , \tag{3.9}$$

$$x\equiv\tfrac{1}{2}(x_1-x_2)\ . \tag{3.10}$$

In these new variables the overlap integral (3.1) becomes

$$c(n_1,n_2)=\frac{1}{\sqrt{\pi}}\int_{-\infty}^{\infty}dx\int_{-\infty}^{\infty}dX\,U_{n_1}(x+\tfrac{1}{2}X)U_{n_2}(-x+\tfrac{1}{2}X)\exp\left(-\frac{\epsilon}{2}(x-x_0)^2\right)\exp\left(-\frac{1}{2\epsilon}(X-X_0)^2\right)\ , \tag{3.11}$$

with

$$X_0\equiv\sqrt{2}(\alpha_1+\alpha_2)\ , \tag{3.12}$$

$$x_0\equiv\frac{1}{\sqrt{2}}(\alpha_1-\alpha_2)\ , \tag{3.13}$$

$$\epsilon\equiv 2e^{-2r}\ . \tag{3.14}$$

We now assume large enough squeezing ($r\gg 1$) that ϵ is sufficiently small to approximate

$$\frac{1}{\sqrt{2\pi\epsilon}}e^{-(X-X_0)^2/2\epsilon} \tag{3.15}$$

as $\delta(X-X_0)$ in Eq. (3.11). A better approximation for $c(n_1,n_2)$ may be obtained by retaining higher-order terms in ϵ, as outlined in Ref. 4, but for our purposes the δ-function approximation is adequate. It enables us to write

$$c(n_1,n_2)\simeq\sqrt{2\epsilon}\int_{-\infty}^{\infty}dx\,U_{n_1}(x+\tfrac{1}{2}X_0)U_{n_2}(-x+\tfrac{1}{2}X_0)\exp\left(-\frac{\epsilon}{2}(x-x_0)^2\right)\ . \tag{3.16}$$

Aside from the Gaussian, the approximation (3.16) is an overlap between two number eigenfunctions of different quantum numbers, one of which is displaced from the origin by $-\frac{1}{2}X_0$ and the other of which is reflected through the origin and then displaced by $\frac{1}{2}X_0$. Indeed, if we neglect the Gaussian, as we may in the large squeezing limit, we may put Eq. (3.16) into the form of a number-state matrix element[14] of a generic displacement operator $\hat{D}(\alpha)\equiv e^{\alpha\hat{a}^\dagger-\alpha^*\hat{a}}$:

$$\begin{aligned}c(n_1,n_2)&\simeq(-1)^{n_2}\sqrt{2\epsilon}\,\langle n_1|\hat{D}(X_0/\sqrt{2})|n_2\rangle\\&=(-1)^{n_2}2e^{-r}\sqrt{p!/q!}\,(X_0/\sqrt{2})^{q-p}L_p^{(q-p)}(X_0^2/2)e^{-X_0^2/4}\ .\end{aligned} \tag{3.17}$$

Except for the irrelevant phase factor $(-1)^{n_2}$, this form of $c(n_1, n_2)$ is the large squeezing limit of the exact probability amplitude (2.14). It allows us to understand why for $X_0 = 0$ (as in Fig. 2) the photon-number probability is concentrated on the main diagonal and has no oscillations.

Returning now to Eq. (3.16), we follow Schleich[5] in developing a semi-classical approximation that employs WKB number-state eigenfunctions and evaluates the integral (3.16) using the method of stationary phase. Our goal is not quantitative accuracy, but rather qualitative physical insight. In the classically allowed region the WKB eigenfunction for a number state with n quanta is given by

$$U_n(x) = \left(\frac{2}{\pi p_n(x)}\right)^{1/2} \cos\left(S_n(x) - \frac{\pi}{4}\right) . \tag{3.18}$$

Here

$$p_n(x) \equiv (r_n^2 - x^2)^{1/2} \tag{3.19}$$

is the momentum at x of a classical trajectory with n quanta, where

$$r_n \equiv \sqrt{2n+1} \tag{3.20}$$

is the trajectory's turning point, or its radius in phase space, and

$$S_n(x) \equiv \int_x^{r_n} dx'\, p_n(x') \tag{3.21}$$

is the phase accumulated from x to r_n.

Under a simultaneous sign change of α_1 and α_2, the photon-counting probability amplitude (2.14) is multiplied by $(-1)^{n_1+n_2}$, thus leaving the joint photon-number probability distribution unchanged. The same symmetry of $c(n_1, n_2)$ is manifested in the exact form (3.11) and in the approximate form (3.16) under a simultaneous sign change of X_0 and x_0. Thus, without loss of generality, we may assume, as we do henceforth, that $X_0 > 0$.

With this assumption the phase-space geometry appropriate for a WKB approximation to the integral (3.16) is depicted in Fig. 4. Associated with the eigenfunction $U_{n_1}(x + \frac{1}{2}X_0)$ is a circle of radius $r_1 \equiv r_{n_1} = \sqrt{2n_1+1}$ centered at $-\frac{1}{2}X_0$; similarly associated with the eigenfunction $U_{n_2}(-x + \frac{1}{2}X_0)$ is a circle of radius $r_2 \equiv r_{n_2} = \sqrt{2n_2+1}$ centered at $\frac{1}{2}X_0$. We must consider three possibilities, which divide the n_1-n_2 plane into three regions:

$$\text{region I: } r_1 + r_2 < X_0 , \tag{3.22}$$

i.e., the circles do not intersect;

$$\text{region II: } |r_1 - r_2| < X_0 < r_1 + r_2 , \tag{3.23}$$

i.e., the circles intersect, but neither lies inside the other;

$$\text{region III: } X_0 < |r_1 - r_2| , \tag{3.24}$$

i.e., one circle lies inside the other.

The boundary between these regions is a parabola,

$$n = \frac{m^2}{2X_0^2} + \tfrac{1}{8}X_0^2 - \tfrac{1}{2} , \tag{3.25}$$

which is symmetric about the main diagonal. In Eq. (3.25) we use sum and difference photon numbers,

$$n \equiv \tfrac{1}{2}(n_1 + n_2) , \tag{3.26}$$

$$m \equiv n_1 - n_2 . \tag{3.27}$$

It is convenient (and consistent with the WKB approximation) to neglect the $-\frac{1}{2}$ on the right-hand side of Eq. (3.25), and we do so throughout the following. The parabola has a turning point at $n_1 = n_2 = \frac{1}{8}X_0^2$ ($n = \frac{1}{8}X_0^2$, $m = 0$), and it contacts the n_1 and n_2 axes at points of tangency, specified by $|m| = 2n = \frac{1}{2}X_0^2$ (i.e., $n_1 = \frac{1}{2}X_0^2$ and $n_2 = 0$ or $n_1 = 0$ and $n_2 = \frac{1}{2}X_0^2$). In Figs. 1(c) and 3(b) we plot the parabola (3.25) and label the three regions for the states considered in those figures. The state of Fig. 2 has $X_0 = 0$, so the parabola degenerates into a line along the main diagonal; region I disappears, region II degenerates to the main diagonal, and region III covers the rest of the n_1-n_2 plane.

In region I the integral (3.16) is small, because at least one of the eigenfunctions is always outside the classically allowed region. Thus we expect that the joint distribution $P(n_1, n_2)$ is small in region I, and we further expect that the first maximum of the joint distribution occurs as the classically allowed regions begin to overlap, which is at or just beyond the parabolic boundary between regions I and II. This picture is confirmed qualitatively by the joint distributions plotted in Figs. 1(b) and 3(a), which have regions of small probability near the origin, shaped like region I, and a first maximum that appears to lie on a parabola. To test the picture a bit more quantitatively, we plot in Figs. 1(c) and 3(b) the actual position of the first maximum and find very good agreement with the parabolic boundary between regions I and II.

In region III also the integral (3.16) is small, because although the classically allowed regions overlap, there is no point of stationary phase, so the integrand oscillates rapidly. Thus we expect $P(n_1, n_2)$ to be small in region III, a picture confirmed qualitatively by the joint distributions plotted in Figs. 2(b) and 3(a). In addition, the plot of first maxima in Fig. 3(b) illustrates strikingly the transition from very low probabilities in region III to higher probabilities in region II as one crosses the parabolic boundary between the two regions.

We implement our semiclassical approximation in region II. Neglecting contributions from the classically forbidden regions and plugging WKB eigenfunctions [Eq. (3.18)] into the approximation (3.16), we find

$$c(n_1,n_2) \simeq \frac{\sqrt{2\epsilon}}{\pi}\int_{X_0/2-r_2}^{r_1-X_0/2} dx\, \frac{e^{-\epsilon(x-x_0)^2/2}}{[p_{n_1}(x+\frac{1}{2}X_0)p_{n_2}(-x+\frac{1}{2}X_0)]^{1/2}} \sin\Phi_{n_1,n_2}(x)\ , \tag{3.28}$$

where we have combined the two cosine functions and discarded a term that oscillates rapidly, and where we define a phase,

$$\Phi_{n_1,n_2}(x) \equiv S_{n_1}(x+\tfrac{1}{2}X_0) + S_{n_2}(-x+\tfrac{1}{2}X_0)\ . \tag{3.29}$$

We now evaluate the integral (3.28) by the method of stationary phase. The stationary phase condition,

$$\left.\frac{\partial\Phi_{n_1,n_2}(x)}{\partial x}\right|_{x=x_s} = 0\ , \tag{3.30}$$

is equivalent to

$$p_{n_1}(x_s+\tfrac{1}{2}X_0) = p_{n_2}(-x_s+\tfrac{1}{2}X_0) \tag{3.31}$$

and has the solution

$$x_s = \frac{r_1^2-r_2^2}{2X_0} = \frac{m}{X_0}\ . \tag{3.32}$$

Equations (3.31) and (3.32) have the simple geometrical interpretation sketched in Fig. 4. Using the solution (3.32), we may rewrite Eq. (3.31) as

$$p_{n_1}(x_s+\tfrac{1}{2}X_0) = p_{n_2}(-x_s+\tfrac{1}{2}X_0) = \sqrt{2}\,(n - m^2/2X_0^2 - \tfrac{1}{8}X_0^2 + \tfrac{1}{2})^{1/2}\ , \tag{3.33}$$

which vanishes on the parabolic boundary (3.25). Using the method of stationary phase, with

$$\left.\frac{\partial^2\Phi_{n_1,n_2}(x)}{\partial x^2}\right|_{x=x_s} = \frac{X_0}{p_{n_1}(x_s+\frac{1}{2}X_0)}\ , \tag{3.34}$$

and then squaring, we find an approximate joint photon-number distribution in region II,

$$P(n_1,n_2) \simeq \frac{4\epsilon}{\pi X_0 p_{n_1}(x_s+\frac{1}{2}X_0)} \exp\left(-\frac{\epsilon}{X_0^2}(m-X_0x_0)^2\right)\sin^2\left(\Phi_{n_1,n_2}+\frac{\pi}{4}\right)\ , \tag{3.35}$$

where the phase (3.29) at the stationary solution,

$$\Phi_{n_1,n_2} \equiv \Phi_{n_1,n_2}(x_s) = S_{n_1}(x_s+\tfrac{1}{2}X_0)+S_{n_2}(-x_s+\tfrac{1}{2}X_0)\ , \tag{3.36}$$

is the cross-hatched area in Fig. 4.

What can we say about the approximate distribution (3.35)? It predicts oscillations, because of the phase Φ_{n_1,n_2}, and it thus permits us to understand the oscillations as due to interference in phase space.[3,5] This interpretation arises from allowing the circle for an eigenstate with n quanta to become a band whose thickness is chosen so that the area of the band is 2π, the quantum in phase space when $\hbar = 1$. Then the integral (3.16) is interpreted[5] as coming from the area of overlap of the two bands in the phase space of Fig. 4; the phase Φ_{n_1,n_2} describes interference between the two areas of overlap—an interference in phase space.

The approximate distribution (3.35) also predicts Gaussian behavior in the difference m. The mean of the Gaussian lies at $m = X_0x_0$, and its half-width is $\frac{1}{2}X_0e^r$. This behavior is confirmed qualitatively by the joint distributions in Figs. 1–3. In particular, it is consistent with the concentration of the joint distribution in Fig. 2(b) along the main diagonal, because $X_0 = 0$ for the state of Fig. 2.

Despite these successes, the semiclassical approximation and its joint distribution (3.35) are poor approximations, not least because it is difficult to estimate errors and to delineate the region of validity, if any. Near the parabolic boundary of region II the joint distribu-

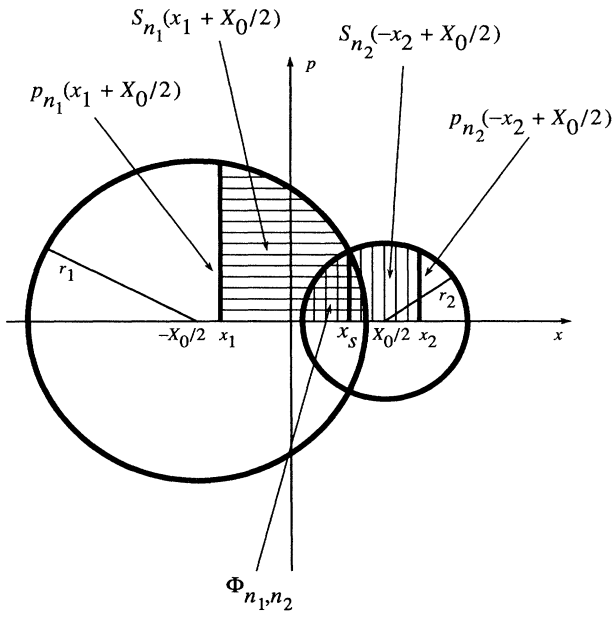

FIG. 4. Phase-space geometry for the semiclassical approximation to the integral (3.16). Associated with the eigenfunction $U_{n_1}(x+\frac{1}{2}X_0)$ is a circle of radius $r_1 = \sqrt{2n_1+1}$ centered at $-\frac{1}{2}X_0$; associated with the eigenfunction $U_{n_2}(-x+\frac{1}{2}X_0)$ is a circle of radius $r_2 = \sqrt{2n_2+1}$ centered at $-\frac{1}{2}X_0$. The momenta $p_{n_1}(x_1+\frac{1}{2}X_0)$ and $p_{n_2}(-x_2+\frac{1}{2}X_0)$ are represented by the labeled vertical lengths. The phases $S_{n_1}(x_1+\frac{1}{2}X_0)$ and $S_{n_2}(-x_2+\frac{1}{2}X_0)$ are represented by the areas delineated by thin horizontal and vertical lines, respectively. The stationary-phase condition (3.31) is met at position x_s. The phase Φ_{n_1,n_2} [Eq. (3.36)] is the area of the cross-hatched region.

tion (3.35) does very poorly, as is evidenced by its blowing up there, the reason being the use of WKB eigenfunctions and the stationary-phase method near classical turning points. The WKB eigenfunctions and the stationary-phase method do better deep inside region II, far from the boundary, but that is precisely where the δ-function approximation that leads to Eq. (3.16) runs into trouble, because the number-state eigenfunctions oscillate very rapidly. Indeed, the joint distribution (3.35) does not decrease nearly fast enough as n increases. In short, the joint distribution (3.35) is mainly a guide to insight, rather than a tool for calculation.

ACKNOWLEDGMENTS

This work was supported in part by the Office of Naval Research (Contract No. N00014-88-K-0042).

[1] For reviews of squeezed light, see R. Loudon and P. L. Knight, J. Mod. Opt. **34**, 709 (1987) and M. C. Teich and B. E. A. Saleh, Quantum Opt. **1**, 153 (1989); see also *Squeezed States of the Electromagnetic Field,* edited by H. J. Kimble and D. F. Walls, special issue of J. Opt. Soc. Am. B **4**, 1453–1741 (1987).

[2] H. P. Yuen, Phys. Rev. A **13**, 2226 (1976).

[3] W. Schleich and J. A. Wheeler, Nature **326**, 574 (1987); J. Opt. Soc. Am. B **4**, 1715 (1987).

[4] W. Schleich, D. F. Walls, and J. A. Wheeler, Phys. Rev. A **38**, 1177 (1988).

[5] For a thorough exegesis of the concept of interference in phase space, see W. Schleich, habilitation thesis, Max-Planck-Institut für Quantenoptik, Garching, Federal Republic of Germany, 1988.

[6] C. M. Caves and B. L. Schumaker, Phys. Rev. A **31**, 3068 (1985); B. L. Schumaker and C. M. Caves, *ibid.* **31**, 3093 (1985).

[7] R. E. Slusher, P. Grangier, A. LaPorta, B. Yurke, and M. J. Potasek, Phys. Rev. Lett. **59**, 2566 (1987).

[8] O. Aytür and P. Kumar, Phys. Rev. Lett. **65**, 1551 (1990).

[9] G. J. Milburn and D. F. Walls, Phys. Rev. A **38**, 1087 (1988).

[10] C. Zhu and C. M. Caves, Phys. Rev. A **42**, 6794 (1990).

[11] S. M. Barnett and P. L. Knight, J. Opt. Soc. Am. B **2**, 467 (1985).

[12] *Handbook of Mathematical Functions,* edited by M. Abramowitz and I. A. Stegun (U.S. GPO, Washington, D.C., 1964), Eq. (22.9.15).

[13] B. L. Schumaker, Phys. Rep. **135**, 317 (1986).

[14] F. A. M. de Oliveira, M. S. Kim, and P. L. Knight, Phys. Rev. A **41**, 2645 (1990).